Partially Carbonized Carbon Fibers as an Improved Multifunctional Structural Battery Electrode

PARTIALLY CARBONISED CARBON FIBRES AS AN IMPROVED MULTIFUNCTIONAL STRUCTURAL BATTERY ELECTRODE

Ruben Tavano[1*], Johanna Xu[1], Claudia Creighton[2], James D. Randall[2], Luke C. Henderson[2], Leif E. Asp[1]

[1]Industrial and Materials Science, Chalmers University of Technology, 41296 Göteborg, Sweden

[2]Institute of Frontier Materials, Deakin University, Geelong Waurn Ponds Campus, VIC 3216, Australia

* Corresponding author (ruben.tavano@chalmers.se)

Keywords: *Carbon fibre; Smart materials; Multifunctionality*

Abstract

Carbon fibres are increasingly explored for use in structural battery electrodes due to their ability to combine mechanical strength and stiffness with electrochemical functionality. The properties of carbon fibres are largely governed by their microstructure, which is shaped by the processing conditions—particularly the carbonisation temperature. This study focuses on exploring how partial carbonisation during manufacture influences the multifunctional performance of carbon fibres. The manufactured fibres are subjected to mechanical and electrochemical tests to evaluate their tensile properties, and reversible capacity. The results confirm previously reported multifunctionality trade-offs: when comparing to conventional intermediate modulus carbon fibres, by reaching a maximum temperature of 900 °C (compared to the usual 1500 °C) the electrochemical capacity increases at the expense of mechanical performance. Up to a 50% reduction in tensile modulus is observed alongside a 40% improvement in electrochemical capacity. These findings highlight the potential to greatly expand the achievable multifunctionality window for carbon fibres by adjusting the maximum carbonisation temperature, enabling a versatile design of active materials for structural energy-storing applications.

Introduction

The development of multifunctional materials is paving the way for significant changes in energy storage solutions for transportation and portable devices. One of the most promising concepts are structural battery composites (SBCs), which combine structural functions with the ability to store electrical energy. By embedding energy storage directly into load-bearing components, such as those in electric vehicles, designers can reduce weight, increase efficiency and consequently extend driving range. Structural battery composites embody this dual functionality, enabling materials to perform as both batteries and composite panels. Typically, a structural battery features a configuration where a thin-ply carbon fibre tow acts as the negative electrode, layered with a separator and a counter electrode[1–6]. These layers are infused with a structural battery electrolyte (SBE), which provides load transfer capabilities and ionic transport[7–11]. Due to their multifunctionality, carbon fibres not only provide structural reinforcement but also serve as lithium hosts and electron conductors.

While the mechanical properties of commercial carbon fibres are well-characterised, owing to their established role in composite reinforcement, their electrochemical behaviour remains less understood. Works by Jacques et al. and Duan et al. helped shed light on how lithium insertion alters the physical and mechanical characteristics of these fibres[12–15]. Additional investigations by Kjell et al. evaluated the electrochemical performance of widely used PAN-based carbon fibres[16], and Hagberg et al. examined the capacity and coulombic efficiency of intermediate modulus (IM) fibres (such as T800 and IMS65) in contrast to high modulus (HM) fibres like M60J, using precise coulometry techniques[17]. IM fibres generally exhibited superior electrochemical capacity, though the exact mechanisms behind this disparity were not initially clear.

Fredi et al. employed high-resolution transmission electron microscopy and in-situ Raman spectroscopy to uncover the underlying lithiation processes in T800, IMS65, and M60J fibres[18]. Their findings revealed that IM fibres behave somehow similarly to amorphous carbon during lithium insertion, with each fibre displaying unique performance characteristics. Conversely, the HM fibre followed a graphite-like staging mechanism, which was hindered by defects in its large crystalline domains. This structural obstruction contributed to its lower lithium capacity. Further insights into the performance differences between IM fibres were offered by Johansen et al., who investigated the role of heteroatoms in the carbon fibre microstructure[19]. They discovered notable variations in nitrogen content: IMS65 contained 20.5% pyridinic and pyrrolic nitrogen compared to just 14.2% in T800. These nitrogen configurations typically appear at defect sites and facilitate lithium coordination, suggesting that the higher concentration of these species in IMS65 may account for its enhanced capacity.

Asp et al. demonstrated the potential of intermediate modulus (IM) carbon fibres for multifunctional energy applications by integrating T800 fibres into a laminated structural battery composite, where the fibres functioned as the negative electrode[20]. Their prototype achieved an energy density of 24 Wh/kg alongside a mechanical stiffness of 25 GPa, exemplifying the material's dual structural and electrochemical roles. More recently, by using carbon fibres coated with lithium iron phosphate as the active material for the positive electrode, Chaudhary et al. managed to realise the first all-fibre structural battery. They boosted the structural battery performance leading to a significant improvement in the mechanical performance, with a tensile modulus of 76 GPa and a slight decrease in the energy density to 30 Wh/kg[21,22].

Despite such advancements, significant challenges remain. Commercially available carbon fibres have traditionally been optimised solely for mechanical properties, particularly strength and stiffness, without consideration for electrochemical functionality. This presents complications for multifunctional applications, not only because critical details such as the precursor materials and processing conditions are often proprietary, but also because the fibres are typically coated with sizing agents whose chemical composition is unknown, potentially interfering with their performance in electrochemical applications.

In an effort to better understand how lithium interacts with carbon fibres and to identify which microstructural characteristics enhance electrochemical performance, Xu et al. and Tavano et al. manufactured custom-made carbon fibres. The same PAN-based precursor was used in both cases, but each study introduced distinct modifications during fibre processing. Xu et al. varied the tensile force applied during the stabilisation stage, while Tavano et al. adjusted the carbonisation temperature profiles. These deliberate alterations allowed them to systematically investigate the effects of processing conditions on the resulting fibre properties. Their findings revealed a fundamental trade-off between mechanical properties and electrochemical performance. As the electrochemical capacity of the fibres improved, a corresponding decline in mechanical performance was observed, highlighting the inherent antagonistic character between these two functional objectives in carbon fibres. Furthermore, it was shown that fibres with a less ordered microstructure, specifically those with reduced crystalline carbon content, smaller crystallite sizes, and increased interlayer spacing within the crystalline regions, exhibited superior lithium storage capabilities. These results suggest that while high structural order favours mechanical strength, a more disordered carbon structure can be advantageous for lithium intercalation, pointing to the need for careful optimisation when designing carbon fibres for multifunctional applications.

In the current study, we investigate a custom-made carbon fibre manufactured only by a partial carbonisation step. The resulting carbonaceous microstructure attributes peculiar properties to the fibres, enabling us to further expand the design window for structural battery composites. Previous studies have focused on HM and IM carbon fibres. HM fibres have high mechanical performance but almost non-existent lithium storing capabilities. IM fibres show a good multifunctionality compromise. With partially carbonised carbon fibres, the mechanical properties are significantly decreased but unmatched reversible

electrochemical capacity is reached. These types of fibres can prove useful for applications that need energy storage at low mechanical requirements, and can guide the development of a new category of multifunctional fibres.

Experimental

Materials: Carbon fibres were produced at Carbon Nexus, Institute for Frontier Materials at Deakin University, Australia, using a research-grade production line. The production process followed similar criteria as in the previous studies by Xu et al. and Tavano et al.[23,24]. The precursor material was a 24 K tow of polyacrylonitrile (PAN) fibres sourced from Bluestar Ltd (China). Following stabilisation, the fibres were subjected to a carbonisation process only in the low temperature carbonisation furnace (LT furnace), reaching a maximum temperature of 900 °C. During production, the fibre line operated at a speed of 30 m/h, resulting in residence times of approximately 2 h in the stabilisation step and 2.5 minutes in the low-temperature carbonisation furnace. Throughout the oxidation phase, the fibres were subjected to an average tension of 2300 cN. This tension was adjusted in the carbonisation stage, with values maintained at 1200 cN during the low-temperature carbonisation. After exiting the LT furnace, the carbon fibres were directed to a winder for collection.

For the electrochemical characterisation, half-cells were assembled. Glass fibre separator (Whatman GF/A, ~260 µm thick), lithium metal foil (99.9%, 0.75 mm thick), lithium bis(trifluoromethanesulfonyl)imide (LiTFSI, anhydrous, 99.99%), propylene carbonate (PC, ≥99%, acid <10 ppm, H_2O <10 ppm), and ethylene carbonate (EC, 99% anhydrous) were all purchased from Sigma Aldrich (USA). The copper foil, nickel foil and silver glue used for the cell assembly were purchased from Ted Pella, Inc. (USA).

Physical properties: Fibre density was assessed using a Ultrapyc 1200e pycnometer (Quantachrome, Austria), with three replicate measurements. The fibre diameter was obtained combining the fibre density with the vibrational analysis conducted via a Favimat+ single fibre tensile test machine (Textechno, Germany) prior to mechanical testing. Conductivity was evaluated via the four-point probe method, with ten measurements carried out to ensure reproducibility and consistency. Surface area measurements were obtained using Brunauer–Emmett–Teller (BET) analysis, conducted on an inverse gas chromatography surface energy analyser (Surface Measurement Systems, UK) with octane gas adsorption at 30 °C. Complementary imaging of the carbon fibre surfaces was performed using a field emission scanning electron microscope LEO-1550 (Zeiss, Germany) to reveal surface texture and morphology.

Raman spectroscopy: Raman spectra were recorded using a WITec alpha300 R spectrometer (WITec GmbH, Germany), equipped with a confocal microscope Zeiss LSM (Zeiss, Germany) and a 50× magnification objective lens Zeiss EC Epiplan (NA = 0.75) (Zeiss, Germany). All measurements were carried out at room temperature (23 °C) using a 532 nm laser excitation source. The laser, focused to approximately 300 nm spot size, enabled detailed analysis of individual carbon fibres. Data acquisition was performed in backscattering geometry, using a 100 µm slit, a 600 lines/mm diffraction grating, and no optical filters. The spectra were collected using a charge-coupled device (CCD) detector. To enhance the signal-to-noise ratio (S/N), each spectrum was composed of 60 accumulations, each with an exposure time of 1 second. Post-processing of the spectra was performed using the software Project FIVE (WITec GmbH, Germany). A linear baseline was subtracted to correct for background fluorescence, and Savitzky-Golay smoothing was applied to further reduce noise. Spectral peaks were analysed in terms of Raman shift, intensity, area, and full width at half maximum (FWHM), using Lorentz function fitting. For visual comparison, all spectra were normalised to the most intense peak.

Mechanical Properties: Mechanical properties, including tensile strength, elastic modulus, and strain to failure, were characterised using single filament tensile testing with a Favimat+ machine (Textechno, Germany), equipped with a 210 cN load cell and a 20 mm gauge length. Tests were performed according

to ASTM D3822-07 at a constant strain rate of 1 mm/min. Seventy-five individual fibres were tested for each fibre type.

Electrochemical properties: Electrochemical characterisation involved the preparation of electrode samples using 24K tows of carbon fibres. To facilitate the electrode performance and repeatability, the tows were divided into two 12K tows prior to assembly. To establish electrical contact, copper strip current collectors were bonded to the carbon fibres using silver paint. Nickel foil was used as a current collector in the counter electrode. The assembled carbon fibre electrodes were dried under vacuum at 50 °C overnight before transfer to an argon-filled glovebox (with H_2O and O_2 levels <1 ppm).

The electrochemical testing employed a two-electrode pouch cell configuration. Lithium metal foil served as both counter and reference electrode. Glass microfiber separator was used to insulate the two electrodes. The liquid electrolyte was then added to the cell prior to sealing it. The complete cell was sealed in a pouch bag prior to testing. Galvanostatic charge/discharge cycles were conducted to determine specific capacity, coulombic efficiency, and first-cycle losses. Testing was carried out on a Neware CT-4008-5V10mA-164 battery cycler (Neware, China). For half-cell cycling studies, the voltage window was set from 0.01 V to 1.50 V versus Li/Li^+. The applied current densities were based on graphite's theoretical capacity (372 mAh g^{-1}), corresponding to 0.05C (for the conditioning cycles), 0.1C, 0.2C, and 0.4C. The sequence included ten cycles at 0.05C, followed by five each at 0.1C, 0.2C and 0.4C, and concluding with twenty-five additional cycles at 0.1C. A resting period of two hours was applied after each charge/discharge phase.

Results and Discussion

For comparison purposes, we report the results of the partially carbonised fibre, labelled PC900, and two IM carbon fibres investigated in previous studies. These are commercially available T800 carbon fibres and the cool temperature profile (CP) carbon fibres from Tavano et al. (which are referred to as fully carbonised (FC) in the coming sections)[24]. The importance of comparing the fibres from this study to the FC fibres lies in the almost identical manufacturing process. The only difference was a passage in the high-temperature carbonisation furnaces for the FC fibres, which made them similar to other IM carbon fibres. This difference attributes peculiar microstructural differences to the two fibres.

Physical Properties:

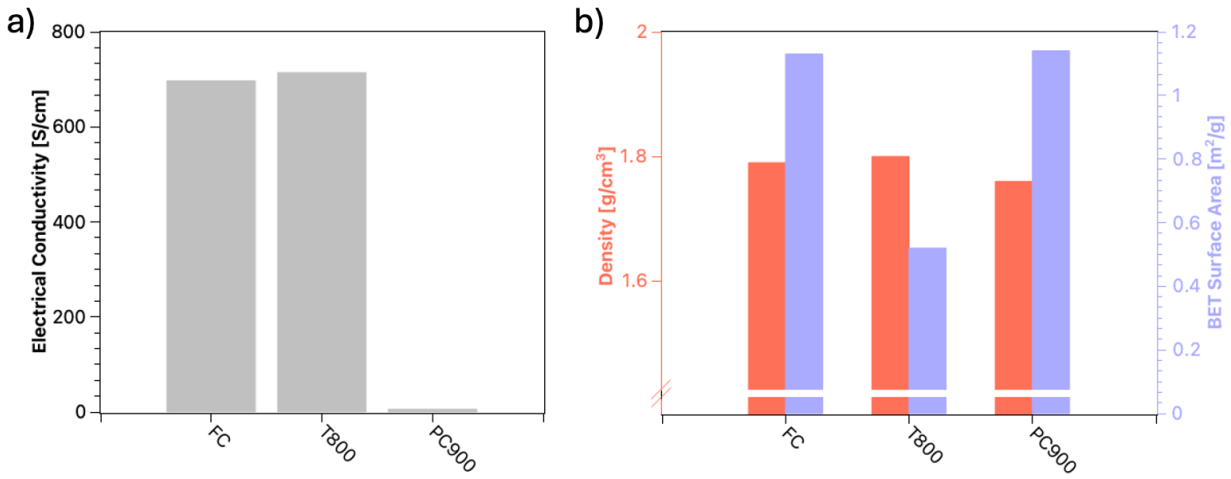

Figure 1 Physical, mechanical and electrochemical properties overview for two IM carbon fibres (FC and T800) and the partially carbonised carbon fibre (PC900). a) Electrical conductivity; b) Density and BET surface area.

Electrical conductivity is needed for energy storage applications since the active material needs to be conductive enough to transport electrons to and from the current collector. No clear requirements in terms of minimum conductivity have been reported in the literature. In Figure 1a, a comparison of the three

fibres is shown for the electrical conductivity. Values more than two orders of magnitude lower were measured for the PC900 fibres compared to the IM fibres.

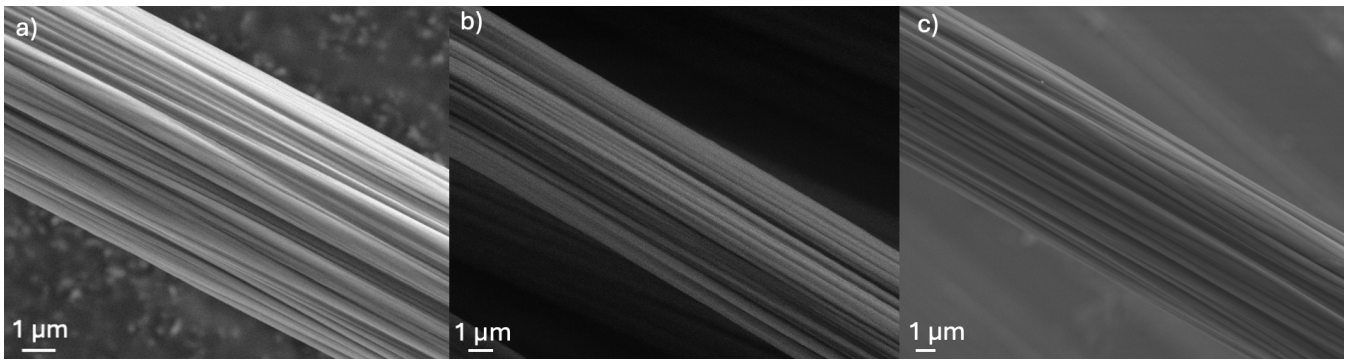

Figure 2. SEM surface images of the three carbon fibres at x10k magnification of the. a) FC fibres from Tavano et al[24]; b) T800 fibres; c) PC900 fibres manufactured in the current study.

A comparison of density and BET surface area for the three fibres is shown in Figure 1b. Comparable densities were measured for the two IM carbon, while slightly lower values were measured for the PC900 fibre. The BET surface area is highly influenced by the type of precursor fibre used for the manufacturing. The values measured for all the fibres were very low, below 1.2 m^2 g^{-1}, and comparable, indicating that the precursor was produced with a similar wet spinning process[25–27]. These results are confirmed by the SEM images shown in Figure 2a-c, where no significant differences are evident. Similar crenulations along the fibre length are visible for all fibre types.

Raman Spectroscopy: The three fibre types were characterised via Raman spectroscopy to obtain information about the carbonaceous microstructure and its possible differences due to the different carbonisation process. Different spectra were obtained for the three fibres, with different intensities of the D and G peaks along with differences in the Raman shift values.

In Figure 3a, the three spectra are shown in the 500-2500 cm^{-1} Raman shift range with a zoomed-in view of the D and G peaks in the inset. Similar G' peaks were observed in all the samples, indicating a low degree of crystallisation, small domains and a turbostratic or amorphous microstructure[28]. For the IM fibres, the intensity is similar for the D and the G peaks, resulting in a ratio between the intensity of the two equal to 1.0 and 0.9 for FC and T800, respectively. This is most likely due to the FC fibre being carbonised at a slightly lower temperature compared to the commercial T800 fibre. For the partially carbonised fibre, the intensity of the D peak is significantly higher, consistent with a more disordered, less graphitised carbonaceous microstructure of this fibre type. In this case, a ratio of 1.2 was calculated between the intensity of the D and G peaks. Additionally, by using the Tuinstra-Koenig approach, the average crystal length in the carbon fibres could be estimated from the peak intensity ratio[29]. Smaller crystallites were calculated for PC900 fibres compared to the two IM fibres with an average crystal length equal to 42 Å, compared to approximately 52 Å for IM fibres. Furthermore, the D and G peaks for the PC900 fibres are slightly shifted towards smaller Raman shifts compared to IM fibres, as can be seen in Figure 3b. This could be caused by residual strains in the microstructure due to the partial carbonisation, as well as a higher amount of heteroatoms and structural disorder[18].

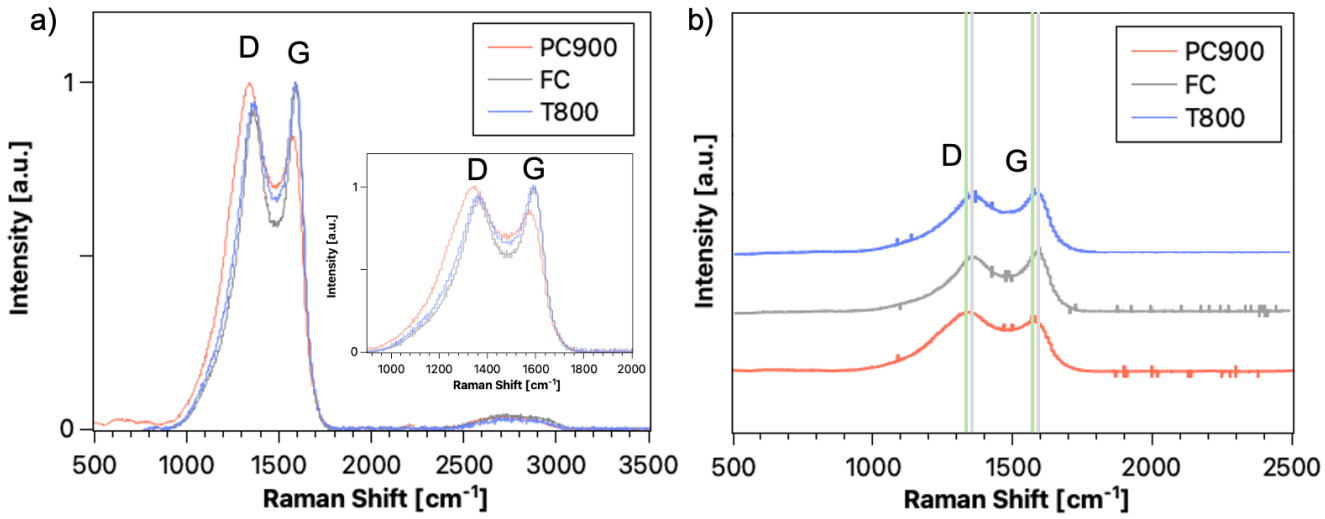

Figure 3 Raman spectroscopy results for IM fibres FC and T800, and partially carbonised fibre PC900. a) Full Raman spectra in the 500-3500 cm^{-1} Raman shift range, with zoomed-in view of the D and G peaks in the inset; b) View of the spectra with movement along the vertical direction. The D and G peaks are slightly shifted towards higher Raman shifts for the IM fibres.

Mechanical Properties: The mechanical properties of carbon fibres are mainly influenced by the tension applied during the stabilisation step and the temperature reached in the carbonisation step[30]. T800 carbon fibres showed the highest mechanical performance with a strain to failure, breaking strength and tensile modulus between 10% and 20% higher than FC fibres. This is most likely due to the maximum reached temperature in the carbonisation step, which was 1300 °C for FC fibres and is unknown for T800 fibres. However, the differences are small when compared to the values measured for PC900 fibres, with a tensile modulus around half that of IM fibres and a breaking strength and strain to failure 40% and 70% lower compared to IM fibres, respectively. All the mechanical properties are shown in Table 1.

Table 1. Mechanical properties for FC, T800 and PC900 carbon fibres.

Sample	Tensile modulus [GPa]	Tensile strength [GPa]	Strain to failure [%]
FC	204.5	2.8	1.4
T800	241.4	3.9	1.7
PC900	99.2	1.0	1.1

Mechanical properties are known to be affected by crystallite size and orientation[18,31]. For partially carbonised carbon fibres, as evidenced by the Raman spectra, smaller crystalline domains were achieved. The difference in the intensity between D and G peaks also suggests that PC900 fibres have a more disordered and less graphitised microstructure, which is further confirmed by the lower mechanical properties compared to IM fibres.

Electrochemical properties: For simplicity purposes and since the differences in the electrochemical behaviour between the FC and T800 fibres were reported to be small, in the following section, the partially carbonised PC900 fibres will only be compared to T800 fibres.

In Figure 4a-f the voltage profiles for charge and discharge for the two fibre types are depicted for various cycles at different current rates. For all the current rates, the PC900 fibres reached a higher specific capacity compared to the IM fibres, here illustrated for the T800 fibre. For the first conditioning cycle in Figure 4a, differences between the two fibres were very conspicuous, especially for the discharging part of the profile. Furthermore, the shapes of the charge and discharge curves were very different, with a

more linear trend observed for PC900. For the other voltage profiles in Figure 4b-e, the differences were more significant for the charging phase, while the discharging phase showed a similar trend. The difference between the curves was also influenced by the current rate used: by increasing the current rate, the voltage curve for T800 fibres got closer to that of PC900 fibres, almost overlapping at a specific current of 150 mA g^{-1} (0.4C rate). In Figure 4f, the reversibility of the behaviour is demonstrated. The 15th and 30th cycles overall, performed at a specific current of 35 mA g^{-1} (0.1C rate), showed an almost perfect overlapping of the curves, indicating reversibility of the lithium insertion/extraction process.

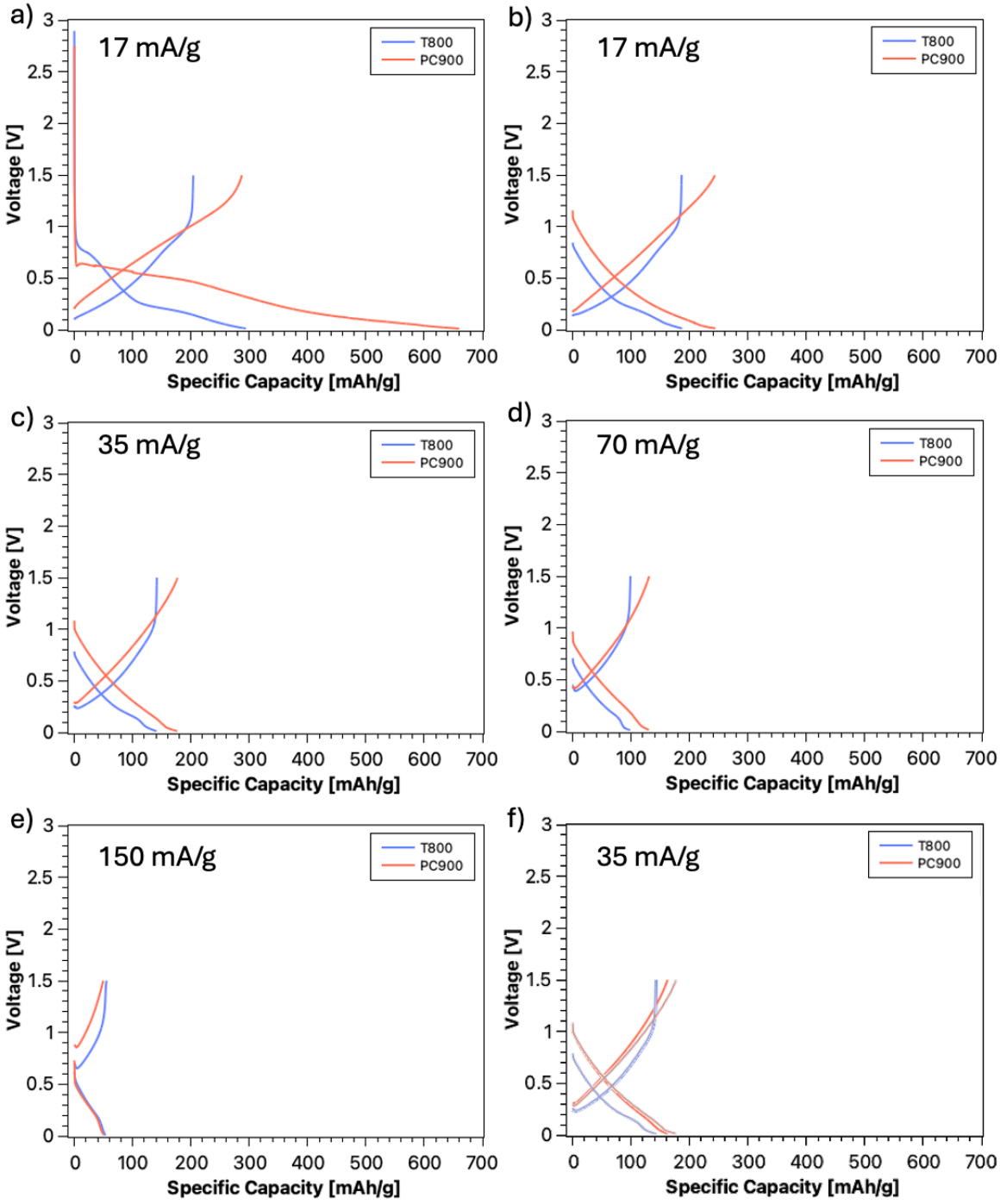

Figure 4. Charge/discharge voltage profiles for T800 and PC900 fibres. a) 1st conditioning cycle at 0.05C rate; b) 10th conditioning cycle at 0.05C rate; c) 5th cycle at 0.1C rate; d) 5th cycle at 0.2C rate; e) 5th cycle at 0.4C rate; f) 30th cycle and 15th cycle (overlayered in grey colour, same as b)) at 0.1C rate.

In Figure 5a, the specific capacities for both fibre types are shown for the different current rates. As expected, with increased current rates, lower specific capacities were measured. However, significant differences in specific capacities were observed between the two fibres, with PC900 performing better at all the current rates and equalling the specific capacity of T800 only at the fastest 0.4C rate. Additionally, the previously mentioned good reversibility of the capacity was observed, as well, when returning to a 0.1C rate after the 25th cycle.

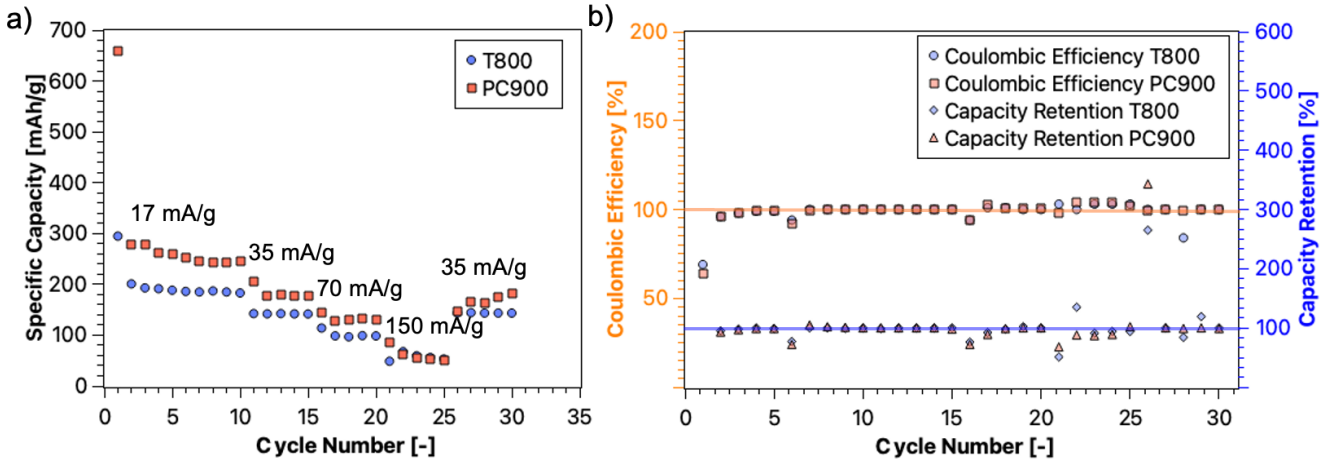

Figure 5 Overall view of the electrochemical cycling results. a) Specific capacity at different current rates at different cycle numbers for T800 and PC900; b) Coulombic efficiency and capacity retention for T800 and PC900.

For the partially carbonised PC900 fibre, an unmatched 1st cycle capacity was measured at more than double the value for T800 fibres. This was accompanied by a much larger 1st cycle loss for PC900 (56% compared to 36%). The reason for this is likely related to more of the inserted lithium ions remaining trapped in the active material due to the more disordered microstructure, as previously reported by Johansen et al.[32]. Furthermore, the results of the electrochemical characterisation are in line with previous studies and the Raman spectroscopy results[18,23,24,33–35]. Previous studies have shown that carbon fibres with a turbostratic microstructure and small crystallite size exhibit lithium storage behaviour similar to that of amorphous carbon. However, unlike fully amorphous materials, these fibres retain some graphitic domains where limited lithium intercalation can still occur. In what is referred to as the "single-layer model," amorphous regions surrounding the disordered crystalline structures impede lithium insertion into graphitic layers. As a result, lithium ions are primarily stored in the amorphous areas and at structural defects such as nanocavities. A prevalence of amorphous domains, more defects and nanocavities, and small crystalline domains in the partially carbonised carbon fibres could explain the better electrochemical performance. In the case of PC900 fibres, higher reversible capacities, with up to 40% better performance for the slower current rates, were observed compared to T800 fibres.

In Figure 5b, the good reversible behaviour for the electrochemical cycling is further evidenced. Comparable Coulombic efficiencies and capacity retentions were measured for both fibres**.** Coulombic efficiency serves as an indicator of how effectively the cell recovers its stored charge, calculated as the proportion of discharge capacity relative to the charge input within a single cycle. In contrast, capacity retention tracks the stability of performance over time by comparing each cycle's discharge capacity to that of the cycle immediately before it. This provides a detailed view of how the cell responds to changing current rates. During the initial cycle, a noticeable decline in efficiency was observed, primarily due to irreversible lithium loss associated with SEI formation and trapped ions. However, from the second cycle onward, Coulombic efficiency rapidly stabilised near 100%, signalling minimal parasitic reactions and excellent reversibility. Capacity retention data further showed that the electrodes maintain consistent performance even when subjected to fluctuations in current rates. Minor dips were correlated with current rate changes but recovered swiftly in the subsequent cycles. This behaviour underscores the

electrochemical reliability of both fibres under dynamic operating conditions. Together, the near-perfect Coulombic efficiency and strong capacity retention present compelling evidence for the durability and reliability of these carbon fibre-based structural anodes in longer-term cycling scenarios. Long-term cycling experiments (i.e. up to 1000 cycles) were not included in this study, in line with previous methodologies that focused on coulombic efficiency as an initial metric. Full-cycle durability testing will be carried out in future investigations once these fibres are integrated into structural full cells, where system-level longevity becomes a central concern[23].

Conclusion

In this study, partially carbonised carbon fibres have been characterised to assess their possible use as active material in a structural negative electrode. Partially carbonised fibres demonstrate an electrical conductivity more than two orders of magnitude lower than IM fibres. Nonetheless, the low conductivity is still sufficient for the electrochemical functioning. The lower temperature used during carbonisation of the partially carbonised fibre resulted in a lower number of graphitic domains and smaller crystallites. As a consequence, the mechanical properties of the partially carbonised fibres were reduced, with a tensile modulus reaching less than half of the IM fibres' value. In contrast, the electrochemical performance highly benefited from the achieved microstructure, with specific capacity values which were up to 40% higher compared to IM fibres. These results confirm what was previously observed, with a clear trade-off in terms of multifunctionality. The results from this study expand the previous results from Xu et al. and Tavano et al., highlighting how the multifunctionality window can be enormously expanded by using less conventional production methods[23,24].

Acknowledgements

The authors would like to thank the following entities for funding this research: United States Air Force (USAF), USA, Award Number FA8655-21-1-7038, Office of Naval Research (ONR), USA, Award Numbers N62909-22-1-2037 and N62909-22-1-2052, Swedish National Space Agency, Contract 2020-00256, Swedish Energy Agency, Contract 46598-1, 2D TECH VINNOVA Competence Center, Contract 2019-00068. This work was partly performed at the Chalmers Material Analysis Laboratory (CMAL).

The authors would also like to thank Mr. John Herron, Dr. Maxime Maghe and Mr. Scott Anderson at Carbon Nexus for manufacturing the carbon fibres analysed in the current study.

References

(1) Asp, L. E.; Greenhalgh, E. S. Structural Power Composites. *Compos. Sci. Technol.* **2014**, *101*, 41–61. https://doi.org/10.1016/j.compscitech.2014.06.020.

(2) Asp, L. E.; Johansson, M.; Lindbergh, G.; Xu, J.; Zenkert, D. Structural Battery Composites: A Review. *Funct. Compos. Struct.* **2019**, *1* (4), 042001. https://doi.org/10.1088/2631-6331/ab5571.

(3) Jin, T.; Singer, G.; Liang, K.; Yang, Y. Structural Batteries: Advances, Challenges and Perspectives. *Mater Today* **2023**, *62*, 151–167. https://doi.org/10.1016/j.mattod.2022.12.001.

(4) Johannisson, W.; Zenkert, D.; Lindbergh, G. Model of a Structural Battery and Its Potential for System Level Mass Savings. *Multifunct. Mater.* **2019**, *2* (3), 035002. https://doi.org/10.1088/2399-7532/ab3bdd.

(5) Meng, C.; Muralidharan, N.; Teblum, E.; Moyer, K. E.; Nessim, G. D.; Pint, C. L. Multifunctional Structural Ultrabattery Composite. *Nano Lett.* **2018**, *18* (12), 7761–7768. https://doi.org/10.1021/acs.nanolett.8b03510.

(6) Moyer, K.; Meng, C.; Marshall, B.; Assal, O.; Eaves, J.; Perez, D.; Karkkainen, R.; Roberson, L.; Pint, C. L. Carbon Fiber Reinforced Structural Lithium-Ion Battery Composite: Multifunctional Power Integration for CubeSats. *Energy Storage Mater* **2020**, *24*, 676–681. https://doi.org/10.1016/j.ensm.2019.08.003.

(7) Cattaruzza, M.; Fang, Y.; Furó, I.; Lindbergh, G.; Liu, F.; Johansson, M. Hybrid Polymer–Liquid Lithium Ion Electrolytes: Effect of Porosity on the Ionic and Molecular Mobility. *J. Mater. Chem. A* **2023**, *11* (13), 7006–7015. https://doi.org/10.1039/D3TA00250K.

(8) Ihrner, N.; Johannisson, W.; Sieland, F.; Zenkert, D.; Johansson, M. Structural Lithium Ion Battery Electrolytes *via* Reaction Induced Phase-Separation. *J. Mater. Chem. A* **2017**, *5* (48), 25652–25659. https://doi.org/10.1039/C7TA04684G.

(9) Schneider, L. M.; Ihrner, N.; Zenkert, D.; Johansson, M. Bicontinuous Electrolytes via Thermally Initiated Polymerization for Structural Lithium Ion Batteries. *ACS Appl. Energy Mater.* **2019**, *2* (6), 4362–4369. https://doi.org/10.1021/acsaem.9b00563.

(10) Larsson, C.; Larsson, F.; Xu, J.; Runesson, K.; Asp, L. E. Effects of Lithium Insertion Induced Swelling of a Structural Battery Negative Electrode. *Composites Science and Technology* **2023**, *244*, 110299. https://doi.org/10.1016/j.compscitech.2023.110299.

(11) Tavano, R.; Spagnol, M.; Al-Ramahi, N.; Joffe, R.; Xu, J.; Asp, L. E. Mechanical Characterisation of a Structural Battery Electrolyte. *Polymer* **2024**, *312*, 127646. https://doi.org/10.1016/j.polymer.2024.127646.

(12) Jacques, E.; H. Kjell, M.; Zenkert, D.; Lindbergh, G. The Effect of Lithium-Intercalation on the Mechanical Properties of Carbon Fibres. *Carbon* **2014**, *68*, 725–733. https://doi.org/10.1016/j.carbon.2013.11.056.

(13) Jacques, E.; Hellqvist Kjell, M.; Zenkert, D.; Lindbergh, G.; Behm, M. Expansion of Carbon Fibres Induced by Lithium Intercalation for Structural Electrode Applications. *Carbon* **2013**, *59*, 246–254. https://doi.org/10.1016/j.carbon.2013.03.015.

(14) Jacques, E.; Kjell, M. H.; Zenkert, D.; Lindbergh, G.; Behm, M.; Willgert, M. Impact of Electrochemical Cycling on the Tensile Properties of Carbon Fibres for Structural Lithium-Ion Composite Batteries. *Compos Sci Technol* **2012**, *72* (7), 792–798. https://doi.org/10.1016/j.compscitech.2012.02.006.

(15) Duan, S.; Iyer, A. H. S.; Carlstedt, D.; Rittweger, F.; Sharits, A.; Maddox, C.; Riemschneider, K.-R.; Mollenhauer, D.; Colliander, M.; Liu, F.; Asp, L. E. Effect of Lithiation on the Elastic Moduli of Carbon Fibres. *Carbon* **2021**, *185*, 234–241. https://doi.org/10.1016/j.carbon.2021.09.037.

(16) Kjell, M. H.; Jacques, E.; Zenkert, D.; Behm, M.; Lindbergh, G. PAN-Based Carbon Fiber Negative Electrodes for Structural Lithium-Ion Batteries. *J. Electrochem. Soc.* **2011**, *158* (12), A1455. https://doi.org/10.1149/2.053112jes.

(17) Hagberg, J.; Leijonmarck, S.; Lindbergh, G. High Precision Coulometry of Commercial PAN-Based Carbon Fibers as Electrodes in Structural Batteries. *J. Electrochem. Soc.* **2016**, *163* (8), A1790. https://doi.org/10.1149/2.0041609jes.

(18) Fredi, G.; Jeschke, S.; Boulaoued, A.; Wallenstein, J.; Rashidi, M.; Liu, F.; Harnden, R.; Zenkert, D.; Hagberg, J.; Lindbergh, G.; Johansson, P.; Stievano, L.; Asp, L. E. Graphitic Microstructure and Performance of Carbon Fibre Li-Ion Structural Battery Electrodes. *Multifunct. Mater.* **2018**, *1* (1), 015003. https://doi.org/10.1088/2399-7532/aab707.

(19) Johansen, M.; Schlueter, C.; Tam, P. L.; Asp, L. E.; Liu, F. Mapping Nitrogen Heteroatoms in Carbon Fibres Using Atom Probe Tomography and Photoelectron Spectroscopy. *Carbon* **2021**, *179*, 20–27. https://doi.org/10.1016/j.carbon.2021.03.061.

(20) Asp, L. E.; Bouton, K.; Carlstedt, D.; Duan, S.; Harnden, R.; Johannisson, W.; Johansen, M.; Johansson, M. K. G.; Lindbergh, G.; Liu, F.; Peuvot, K.; Schneider, L. M.; Xu, J.; Zenkert, D. A Structural Battery and Its Multifunctional Performance. *Adv Energy Sustain Res* **2021**, *2* (3), 2000093. https://doi.org/10.1002/aesr.202000093.

(21) Chaudhary, R.; Chetry, A.; Xu, J.; Xia, Z.; Asp, L. E. Structural Positive Electrodes Engineered for Multifunctionality. *Advanced Science* **2024**, *11* (33), 2404012. https://doi.org/10.1002/advs.202404012.

(22) Chaudhary, R.; Xu, J.; Xia, Z.; Asp, L. E. Unveiling the Multifunctional Carbon Fiber Structural Battery. *Advanced Materials* **2024**, *36* (48), 2409725. https://doi.org/10.1002/adma.202409725.

(23) Xu, J.; Creighton, C.; Johansen, M.; Liu, F.; Duan, S.; Carlstedt, D.; Mota-Santiago, P.; Lynch, P.; Asp, L. E. Effect of Tension during Stabilization on Carbon Fiber Multifunctionality for Structural Battery Composites. *Carbon* **2023**, *209*, 117982. https://doi.org/10.1016/j.carbon.2023.03.057.

(24) Tavano, R.; Xu, J.; Creighton, C.; Liu, F.; Dharmasiri, B.; Henderson, L. C.; Asp, L. E. Influence of Carbonisation Temperatures on Multifunctional Properties of Carbon Fibres for Structural Battery Applications. *Batteries & Supercaps* **2024**, *7* (8), e202400110. https://doi.org/10.1002/batt.202400110.

(25) Minus, M.; Kumar, S. The Processing, Properties, and Structure of Carbon Fibers. *JOM* **2005**, *57* (2), 52–58. https://doi.org/10.1007/s11837-005-0217-8.

(26) Zhang, S.; Wang, R.; Liao, Y. A Comparative Study of Two Kinds of T800 Carbon Fibers Produced by Different Spinning Methods for the Production of Filament-Wound Pressure Vessels. *New Carbon Materials* **2019**, *34* (6), 578–586. https://doi.org/10.1016/S1872-5805(19)60033-8.

(27) Liu, C.; Miao, L.; Zhao, R.; Yang, F.; Unnikrishnan, V.; Rana, R.; Deng, N.; Ghandehari Ferdowsi, M. R.; Chao, Q.; Kang, W.; Razal, J. M.; Miao, L.; Naebe, M.; Li, Q. In-Situ Fabrication of Multifunctional N-Doped Hybrid Carbon Nanotube@carbon Fiber by Recycling Gaseous Effluents of Carbon Fiber Production. *Carbon* **2022**, *193*, 368–380. https://doi.org/10.1016/j.carbon.2022.03.046.

(28) Melanitis, N.; Tetlow, P. L.; Galiotis, C. Characterization of PAN-Based Carbon Fibres with Laser Raman Spectroscopy: Part I Effect of Processing Variables on Raman Band Profiles. *JOURNAL OF MATERIALS SCIENCE* **1996**, *31* (4), 851–860. https://doi.org/10.1007/BF00352882.

(29) Tuinstra, F.; Koenig, J. L. Raman Spectrum of Graphite. *The Journal of Chemical Physics* **1970**, *53* (3), 1126–1130. https://doi.org/10.1063/1.1674108.

(30) Park, S.-J. Precursors and Manufacturing of Carbon Fibers. In *Carbon Fibers*; Park, S.-J., Ed.; Springer Series in Materials Science; Springer: Singapore, 2018; pp 31–67. https://doi.org/10.1007/978-981-13-0538-2_2.

(31) Johnson, D. J. Structure-Property Relationships in Carbon Fibres. *J. Phys. D: Appl. Phys.* **1987**, *20* (3), 286–291. https://doi.org/10.1088/0022-3727/20/3/007.

(32) Johansen, M.; Singh, M. P.; Xu, J.; Asp, L. E.; Gault, B.; Liu, F. Unravelling Lithium Distribution in Carbon Fibre Electrodes for Structural Batteries with Atom Probe Tomography. *Carbon* **2024**, 119091. https://doi.org/10.1016/j.carbon.2024.119091.

(33) Endo, M.; Nishimura, Y.; Takahashi, T.; Takeuchi, K.; Dresselhaus, M. S. Lithium Storage Behavior for Various Kinds of Carbon Anodes in Li Ion Secondary Battery. *J Phys Chem Solids* **1996**, *57* (6), 725–728. https://doi.org/10.1016/0022-3697(95)00339-8.

(34) Endo, M.; Kim, Y. A. Chapter 25 - Applications of Advanced Carbon Materials to the Lithium Ion Secondary Battery. In *Carbon Alloys*; Yasuda, E., Inagaki, M., Kaneko, K., Endo, M., Oya, A., Tanabe, Y., Eds.; Elsevier Science: Oxford, 2003; pp 417–433. https://doi.org/10.1016/B978-008044163-4/50025-5.

(35) Endo, M.; Kim, C.; Karaki, T.; Fujino, T.; Matthews, M. J.; Brown, S. D. M.; Dresslhaus, M. S. In Situ Raman Study of PPP-Based Disordered Carbon as an Anode in a Li Ion Battery. *Synthetic Metals* **1998**, *98* (1), 17–24. https://doi.org/10.1016/S0379-6779(98)00141-6.